Evolution of ferromagnetism in orthorhombic perovskites $Sr_{1-x}Pb_xRuO_3$

J.-G. Cheng, J.-S. Zhou,* and J. B. Goodenough
Texas Materials Institute, University of Texas at Austin, Austin, Texas 78712, USA
(Received 14 December 2009; revised manuscript received 17 March 2010; published 8 April 2010)

We report the high-pressure synthesis of the whole series of orthorhombic perovskites $Sr_{1-x}Pb_xRuO_3$ ($0.0 \leq x \leq 1.0$). The high-pressure products have been characterized by x-ray powder diffraction. Systematic measurements of magnetic and transport properties permit us to establish a detailed phase diagram that includes the evolution of the ferromagnetic phase and a phase transition to an orthorhombic phase with the *Imma* space group at low temperature for the compositions close to $PbRuO_3$. More importantly, we have observed quantum critical phenomena in transport properties as a quantum critical point is reached by reducing T_c to zero. We have also made comparisons of magnetic and transport properties between the $Sr_{1-x}M_xRuO_3$ systems with M=Pb, Ca, and Ba.

DOI: 10.1103/PhysRevB.81.134412 PACS number(s): 71.30.+h, 72.15.Jf

I. INTRODUCTION

The origin of ferromagnetism in the orthorhombic perovskite $SrRuO_3$ is a long-standing problem in the field of condensed-matter physics. In contrast to the weak itinerant-electron ferromagnetism, as in $ZrZn_2$,[1] for example, where only a small fraction of electrons in the conduction band are magnetized, the saturation moment of $SrRuO_3$ at 5 K is close to, but never reaches, the spin-only value even under a magnetic field as high as 44 T.[2] This observation has led to a picture of band electronic states responsible for metallic conduction coexisting with localized spin states. Ferromagnetism would then be due to an indirect exchange interaction between localized spins and itinerant electrons. On the other hand, the critical behavior near T_c in $SrRuO_3$ was found to be close to a mean-field model,[3] which would suggests an itinerant-electron ferromagnetism occurring in this compound. A systematic study[4] of the critical behavior as a function of Ca or Ba substitution or hydrostatic pressure, however, has revealed that $SrRuO_3$ is located at the transition from a convex curvature to a concave curvature in the Arrott plot of the magnetization. The linearity observed in the Arrott plot may have little to do with an itinerant-electron ferromagnetism. A study of the evolution of ferromagnetism in the $Sr_{1-x}Pb_xRuO_3$ system should shed further light on this question.

The relatively small orthorhombic distortion in $SrRuO_3$ makes it nearly optimal for the indirect exchange interaction. The structural distortion can be further reduced by Ba substitution. However, the size variance associated with the chemical substitution plagues this attempt. The broader bandwidth in cubic $BaRuO_3$ reduces the Curie temperature significantly.[5] Ca substitution not only introduces the size variance effect on T_c but it also increases the octahedral-site rotations and Ru-O bond-length splitting. As Ca substitution increases, ferromagnetism is gradually destroyed similar to the dilution model established by Griffiths.[6]

Since Pb^{2+} is slightly larger than Sr^{2+}, the orthorhombic $PbRuO_3$ should have smaller structural distortions than those of $SrRuO_3$. However, the perovskite $PbRuO_3$ is not ferromagnetic down to 1.5 K. A recent neutron-diffraction study at low temperatures has shown that the orthorhombic $PbRuO_3$ undergoes a phase transition to the *Imma* phase at $T_t \approx 90$ K.[7] We have clarified that the phase transition does not alter the metallic ground state and that broadening of the conduction bandwidth due to hybridization between Pb 6*s* and Ru 4*d* orbitals plays a leading role in suppression of the ferromagnetism.[8]

The orthorhombic $PbRuO_3$ is the end member of the system $Sr_{1-x}Pb_xRuO_3$. A phase diagram is badly needed in order to demonstrate the evolution from ferromagnetic $SrRuO_3$ to paramagnetic $PbRuO_3$ and how the low-temperature *Imma* phase develops. In an early report,[9] Kafalas and Longo had mentioned that the Curie temperature falls rapidly with increasing x and vanishes at $x \approx 0.5$. No data of T_c versus x and magnetic and transport properties were provided in that report. In this paper, we report a systematic study of the entire system $Sr_{1-x}Pb_xRuO_3$ ($0 \leq x \leq 1$) that includes transport and magnetic properties as well as the room-temperature crystal structure. We have also made a side-by-side comparison between the effect of Pb substitution and that of Ca and Ba substitutions; the comparison distinguishes clearly the electronic hybridization from the steric effect in Pb-substituted samples and reveals the presence of a quantum critical point (QCP) where broadening of the conduction band reduces T_c to 0 K.

II. EXPERIMENTAL DETAILS

With a synthesis procedure similar to that used to prepare $Sr_{1-z}Ca_zRuO_3$, i.e., firing a stoichiometric mixture of $SrCO_3$, PbO, and Ru powders at 1000 °C for 2 days in air, we always obtained a mixture of perovskite and pyrochlore phases for all compositions of $Sr_{1-x}Pb_xRuO_3$ ($0 < x \leq 1$). The perovskite samples were synthesized under high pressure and high temperature (HPHT) in a Walker-type multianvil module (Rockland Research) from a mixture of perovskite and pyrochlore phases as the starting materials. The starting materials were pressed into small pellets and loaded in a Pt capsule ($\varnothing = 1.68$ mm and $L \sim 3.0$ mm). The whole assembly for high-pressure synthesis is shown in Fig. 1. In a typical HPHT experiment, a MgO (EL=14) octahedron with integrated fin was first compressed to the desired pressure ($4 \leq P \leq 10$ GPa) by eight truncated tungsten-carbide cubes

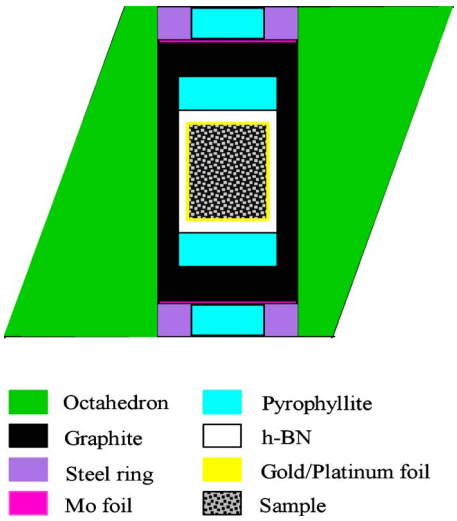

FIG. 1. (Color online) The assembly for high-pressure synthesis in a Walker multianvil press.

with TEL=8 mm; then the temperature at the sample was raised to 1300–1400 °C, depending on the composition, for 30 min before quenching to room temperature. Finally, the pressure was released slowly; it typically takes overnight. High-pressure synthesis is not necessary to make $Sr_{1-z}Ca_zRuO_3$. We made a few compositions in this series under high pressure in order to obtain highly dense samples for transport measurements.

All samples were examined with powder x-ray diffraction (XRD) at room temperature with a Philips X'pert diffractometer (Cu $K\alpha$ radiation). Lattice parameters were obtained by using either the least-squares analysis with the software JADE or the profile fitting with FULLPROF. Magnetic properties were measured with a superconducting quantum interference device magnetometer (Quantum Design). A four-probe method was used to measure the resistivity. Thermoelectric power measurements were performed in a homemade setup.

III. RESULTS AND DISCUSSION

A. Crystal structure

The XRD patterns at room temperature of perovskites $Sr_{1-x}Pb_xRuO_3$ $(0.0 \le x \le 1.0)$, which are displayed in Fig. 2(a). are nearly identical and all major peaks can be indexed with the orthorhombic *Pbnm* space group. As marked by stars in Fig. 2(a), some samples contain a small amount of RuO_2 impurity (<2%). The RuO_2 concentration versus x is shown in Fig. 2(b). No clear trend in RuO_2 impurity versus x was found, which indicates that the temperature window for synthesizing a phase-pure high-pressure product is very narrow in this case. Lattice parameters from refining the XRD of Fig. 2(c) are in good agreement with those reported by Kafalas and Longo. Before discussing the change in lattice parameters as a function of x for Pb, we introduce first the same plot of lattice parameters versus z and y for Ca and Ba substitutions in Fig. 3. A comprehensive structural study of the series $Sr_{1-z}Ca_zRuO_3$ has been done by Kobayashi *et al.*[10] What we plot in Fig. 3 is highly consistent with the data of

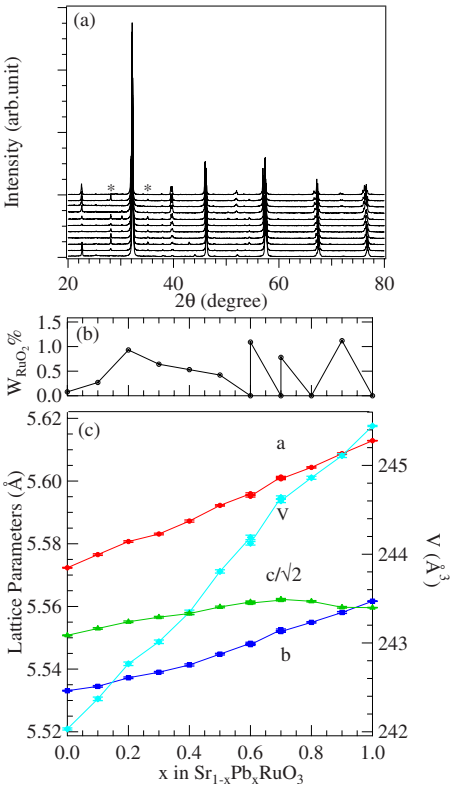

FIG. 2. (Color online) (a) X-ray powder diffraction of orthorhombic $Sr_{1-x}Pb_xRuO_3$; the peak locations marked by stars are from the RuO_2 phase; (b) the concentration of RuO_2 in the high-pressure products as a function of x; (c) lattice parameters and cell volume as a function of x.

Kobayashi *et al.* for the Ca-substituted samples. We have added in Fig. 3 the data of Ba substitution, which shows a complete structural evolution from the orthorhombic *Pbnm* phase all the way to the cubic $Pm\bar{3}m$ phase as the geometric tolerance factor $t \equiv (A\text{-O})/\sqrt{2}(\text{Ru-O})$ increases, where A-O and Ru-O are the equilibrium bond lengths of A-site cation to oxygen and Ru to oxygen, respectively.

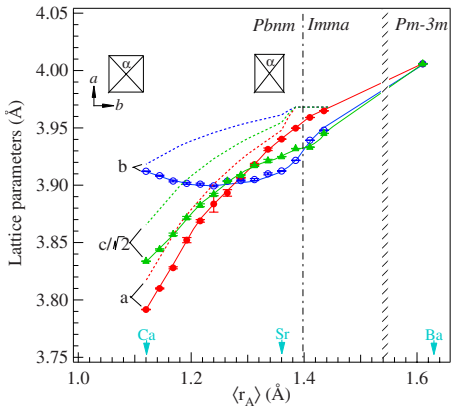

FIG. 3. (Color online) Lattice parameters as a function of the averaged cation size on the A site of perovskites $ARuO_3$ ($A = Ca_{1-i}Sr_i, Sr_{1-j}Ba_j$). Lattice parameters in orthorhombic phases are converted into the primary cell by a factor $1/\sqrt{2}$ in order to compare with that of cubic $BaRuO_3$.

The perovskites $A\mathrm{RuO_3}$ undergo a structural evolution within the *Pbnm* space group and a phase transition to another orthorhombic phase (*Imma*) before the cubic phase ($Pm\bar{3}m$) is reached as the *A*-cation size increases from Ca to Ba. In the orthorhombic phase with the *Pbnm* space group, the cooperative octahedral-site rotation, which is primarily around the *b* axis of the orthorhombic cell, results in $b > c/\sqrt{2} > a$ for rigid $\mathrm{RuO_{6/2}}$ octahedra. The evolution of lattice parameters as a function of the average *A*-cation size $\langle r_A \rangle$ can be well simulated by the software SPUDS (Ref. 11) for the $R^{3+}M^{3+}\mathrm{O_3}$ perovskites. As shown by dashed lines in Fig. 3, however, this simulation does not predict a correct trend of lattice parameters versus $\langle r_A \rangle$ for the perovskites $A\mathrm{RuO_3}$. Although it gives the correct order of $b > c/\sqrt{2} > a$ for $\mathrm{CaRuO_3}$, the predicted *b* versus $\langle r_A \rangle$ deviates from the experimental data from the beginning. The program no longer works for a tolerance factor $t > 1$. While the composition $\mathrm{Sr_{0.9}Ba_{0.1}RuO_3}$ has the orthorhombic structure, the program predicts a cubic phase for this composition. The problem is that the valence-sum value for both Sr^{2+} and Ba^{2+} in the *A* sites used in the SPuDs is slightly larger than their actual size in crystals.

As illustrated systematically in the $A^{3+}B^{3+}\mathrm{O_3}$ perovskites,[12] the $b > a$ deviates from the prediction of SPuDs as the *A*-cation size r_A passes a critical value and eventually crosses to $b < a$ as r_A further increases. The same situation occurs in $A^{2+}\mathrm{Ru^{4+}O_3}$ (A=Ca, Sr, Ba) as is shown in Fig. 3. The anomalous evolution of lattice parameters versus $\langle r_A \rangle$ is due to an octahedral-site distortion with an α angle (see the definition in Fig. 3) less than 90°. There are two important consequences of this kind of octahedral-site distortion: (a) the formula with an assumption of rigid octahedra and using lattice parameters as input parameter,[13] for calculating the $(180° - \phi)$ Ru-O-Ru bond angle is no longer valid; (b) since the *t*-orbital degeneracy is lifted by the intrinsic distortion, the orbital angular momentum in the localized t^4e^0 configuration on the octahedral-site Ru^{4+} is suppressed or reduced significantly. As shown in what follows, the physical properties do not show any anomalies at the crossover of *b* and *a* since the intrinsic site distortion already occurs in the end member $\mathrm{CaRuO_3}$. As monitored by the difference $a-b$, the α angle decreases further as r_A increases. The phase transition to the *Imma* phase is a way for the structure to relieve this local strain. As a matter of fact, the maximum $a-b$ indeed occurs near the *Pbnm*/*Imma* phase boundary.[14,15] Another remarkable change at the phase boundary is a crossover from $c/\sqrt{2} > b$ in the *Pbnm* phase to $c/\sqrt{2} < b$ in the *Imma* phase.

Now we are in the position to discuss the lattice parameters of $\mathrm{Sr_{1-x}Pb_xRuO_3}$ in Fig. 2. Since the r_A of Pb^{2+} is slightly larger than that of Sr^{2+}, the effect of Pb substitution should be similar to that of Ba substitution shown in Fig. 3; $r_A(\mathrm{Pb^{2+}}) \approx 1.4$ Å is at the *Pbnm*/*Imma* phase boundary. Within the range $1.36 < \langle r_A \rangle < 1.4$ Å, Ba substitution reduces $a-b$ slightly. In contrast, $a-b$ increases continuously as *x* increases all the way to $\mathrm{PbRuO_3}$ in Fig. 2. A high-pressure structural study of $\mathrm{PbRuO_3}$ has shown a continuous increase of $a-b$ up to 7 GPa.[8] These results indicate that Pb^{2+} substitution is not as simple as expected from the steric effect. Another important observation from Fig. 2 is that, in contrast to the Ba substitution of Fig. 3, a crossover from $c/\sqrt{2} > b$ to $c/\sqrt{2} < b$ occurs between $x = 0.9$ and 1.0 within the *Pbnm* phase. As far as we know, a $c/\sqrt{2} < a$ *and* b cannot result from intrinsic structural distortions of an orthorhombic perovskite with the *Pbnm* space group. In the orthorhombic $\mathrm{LaMnO_3}$, a $c/\sqrt{2} < a$ *and* b is due to the long-range cooperative Jahn-Teller distortion. The anomalously small $c/\sqrt{2}$ relative to *b* and *a* found in $\mathrm{PbRuO_3}$ is, we believe, related to the hybridization between Pb 6*s* and Ru 4*d* orbitals. This structural anomaly also serves as a precursor to the unusual phase transition to a distinguishable low-temperature *Imma* phase where $c/\sqrt{2}$ is further reduced.

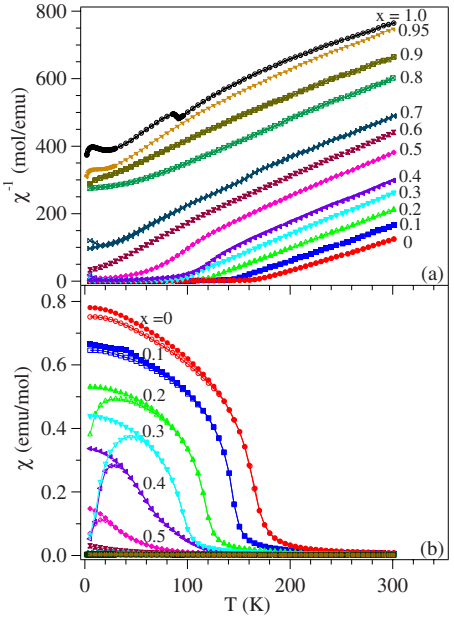

FIG. 4. (Color online) Temperature dependence of (a) the inverse magnetic susceptibility χ^{-1} and (b) χ of $\mathrm{Sr_{1-x}Pb_xRuO_3}$. All plot of $\chi(T)$ for the samples $x > 0.5$ cannot be distinguished in (b).

B. Magnetic properties

The magnetic susceptibility $\chi(T)$ of the whole series $\mathrm{Sr_{1-x}Pb_xRuO_3}$ is shown in Fig. 4. The $\chi(T)$ data for both end members are consistent with those in the literature.[7,8] Fitting these paramagnetic curves to a Curie-Weiss (CW) law gives the Weiss constant θ_{CW} and μ_{eff}; their evolutions as a function of *x* for Pb are plotted in Fig. 5. The Curie temperature T_c of the system is progressively reduced as *x* increases and vanishes near $x = 0.5$. Coincidently, θ_{CW} changes sign from positive to negative at the same composition and the μ_{eff}, which is slightly larger than the spin-only value at $x = 0$, exhibits a minimum near $x = 0.5$. The ultimate issue is why the ferromagnetic phase is suppressed while the structural distortion is gradually reduced as *x* increases. This issue is further addressed below in connection with the systematic study of transport properties. We introduce here a comparison of the magnetic properties among the Ca, Ba, and Pb substitutions.

How the Ca substitution suppresses the ferromagnetic phase in $\mathrm{SrRuO_3}$ remains controversial. We approached this

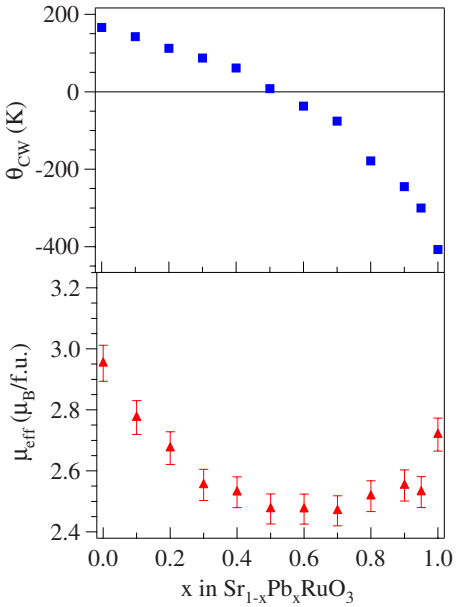

FIG. 5. (Color online) The Weiss constant θ_{CW} and the effective magnetic moment μ_{eff} as a function x in perovskites $Sr_{1-x}Pb_xRuO_3$.

issue by studying the evolution of the paramagnetic susceptibility as a function of Ca substitution. The $\chi(T)$ for our samples $Sr_{1-z}Ca_zRuO_3$ in Fig. 6 is consistent with those in the literature.[2,16–18] A Curie-Weiss law is fulfilled in $SrRuO_3$ in the paramagnetic phase before critical fluctuations set in as T_c is approached. An important feature developed for the Ca-substituted samples is a gradual slope change in the $\chi(T)$ at $T>T_c$, which has the curvature just opposite to that due to critical fluctuations. The same anomaly has been observed in the paramagnetic phase of manganites. However, the feature becomes obvious only for measurements under a weak magnetic field in the case of manganites. Salamon *et al.*[19] have interpreted the anomaly of $\chi(T)$ in the paramagnetic phase of manganites in the context of a Griffiths phase.[6] T_G is defined as the temperature where $\chi(T)$ deviates from the CW law. The regime between T_c and T_G is the Griffiths phase in

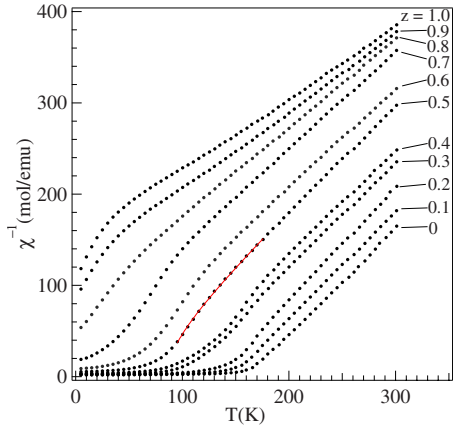

FIG. 6. (Color online) Temperature dependence of the inverse magnetic susceptibility of perovskites $Sr_{1-z}Ca_zRuO_3$. Superimposed on the data for the sample $z=0.5$ is a curve fitting to the formula $\chi^{-1}\sim(T-T_c)^{1-\lambda}$, with $T_c=85.24$ K and $\lambda=0.336$.

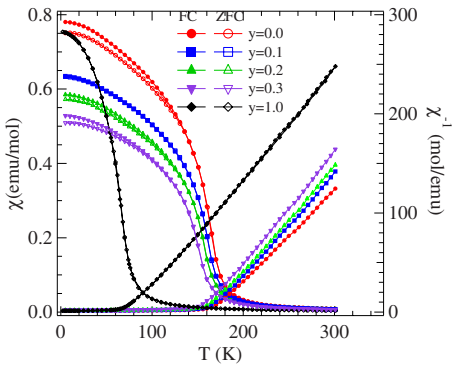

FIG. 7. (Color online) Temperature dependence of magnetic susceptibility χ and χ^{-1} of perovskites $Sr_{1-y}Ba_yRuO_3$.

which the inverse magnetic susceptibility can be described by $\chi^{-1}(T)\propto(T-T_c)^{1-\lambda}$, where λ is positive and less than 1. As superimposed in Fig. 6, the formula fits well the $\chi^{-1}(T)$ for the sample $x=0.5$, for example. The same feature for the Griffiths phase also appears in the $\chi^{-1}(T)$ of Pb-substituted samples with much reduced T_c. Although the characteristic $\chi^{-1}(T)$ for the Griffiths phase appears in both Pb- and Ca-substituted $SrRuO_3$, their T_G do not match the maximum T_c in the system, which is different from the classic phase diagram drawn originally by Griffiths. Nevertheless, there is no doubt that the suppression of the ferromagnetic phase in both Ca- and Pb-substituted $SrRuO_3$ is related to dilution by a nonmagnetic phase. In sharp contrast, Ba substitution in $SrRuO_3$ does not introduce any dilution-related feature in $\chi(T)$ of the paramagnetic phase. Instead, as shown in Fig. 7, the CW law is fulfilled in $\chi(T)$ for all samples $Sr_{1-y}Ba_yRuO_3$ as T_c is reduced from 160 K in $SrRuO_3$ to about 60 K in $BaRuO_3$. Both Pb and Ba substitutions play a similar role in reducing the structural distortions. However, it is the orbital hybridization between Pb^{2+} and Ru^{4+} in Pb-substituted samples that destroys the ferromagnetic phase in $Sr_{1-x}Pb_xRuO_3$.

C. Transport properties

Figure 8 shows the temperature dependence of resistivity and their derivative to temperature of samples $Sr_{1-x}Pb_xRuO_3$. The result for $SrRuO_3$ is closer to that for a single crystal[16,20] than to that of ceramic samples[17] in the literature. We have reported $\rho(T)$ of $PbRuO_3$ at ambient pressure measured in a high-pressure chamber; the result is a bit noisy at low temperatures, probably due to contact with the pressure medium. The result was reproducible as the sample was measured again in a regular sample holder. All samples are metallic down to 5 K; a small upturn at low temperatures of resistivity for the $x=0.1$ sample may be caused by some impurity phase. The ferromagnetic transition in $SrRuO_3$ induces a slope change in the curve of ρ versus T, which can be seen much more clearly in the curve of $d\rho/dT$ versus T. This anomaly moves to lower temperatures and gradually fades away as x increases. On the other hand, the structural transition from the *Pbnm* to the *Imma* phase as temperature lowers through T_d causes an abrupt jump of the resistivity in $PbRuO_3$. The resistivity in the *Imma* phase exhibits a much

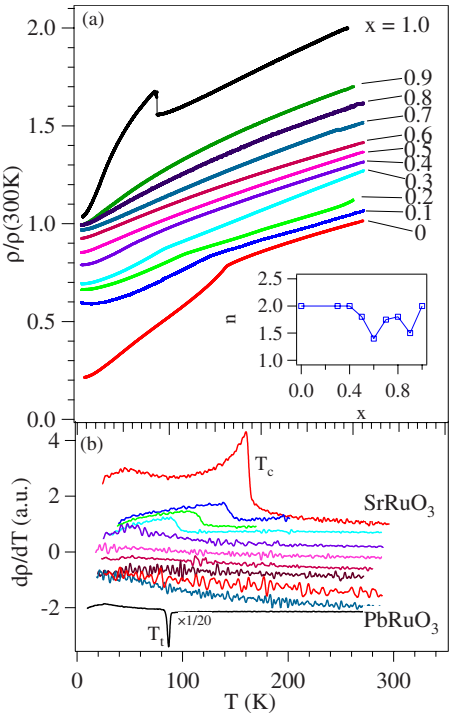

FIG. 8. (Color online) Temperature dependence of resistivity ρ and $d\rho/dT$ of perovskites $Sr_{1-x}Pb_xRuO_3$. All resistivity curves except for the sample $x=0$ have been shifted vertically for clarification. Inset: exponential n in the power law $\rho=\rho_0+T^n$ versus x.

steeper temperature dependence. A power-law analysis of the low-temperature resistivity gives the dependence of exponent n in $\rho=\rho_0+T^n$ versus x shown as an inset of Fig. 8. Both end members show well-defined Fermi-liquid behavior with $n=2$. The non-Fermi-liquid behavior at the first minimum in the plot of n versus x near $x=0.6$ appears to be associated with a quantum critical point as the Curie temperature is suppressed to zero. The second minimum in n versus x is perhaps related to critical fluctuations near the structural transition at T_d which vanishes near $x=0.9$.

The temperature dependence of thermoelectric power for samples $Sr_{1-x}Pb_xRuO_3$ and $Sr_{1-z}Ca_zRuO_3$ are shown in Fig. 9(a). As reported previously,[8] the structural transition at T_t induces an abrupt drop of thermoelectric power followed by a broad minimum in $PbRuO_3$. This broad minimum has been attributed to the phonon-drag effect. Similar features characteristic of the *Imma* phase can still be seen in $x=0.90$ and 0.95 samples of Fig. 10. The transition at T_t in the $x=0.95$ sample, as monitored by an abrupt drop of S, is suppressed under high pressure, which is consistent with the T_t reduction under high pressure observed in $PbRuO_3$.[8] For the samples $x\leq 0.8$, the *Pbnm* phase remains stable to the lowest temperature and a positive hump in S with a maximum near 20 K appears; the enhancement lasts over a broad range of the samples of $Sr_{1-x}Pb_xRuO_3$ and fades away in $SrRuO_3$. No such feature was observed in any Ca-substituted sample. The low-temperature enhancement of thermoelectric power in a metallic phase is normally due to the phonon-drag effect. However, it is highly unusual that the enhancement near 20 K does not maximize at the end members where the Fermi-liquid behavior is well defined from the resistivity measure-

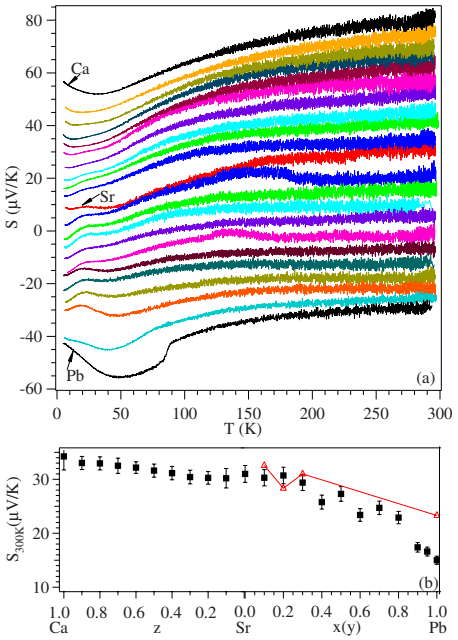

FIG. 9. (Color online) (a) Temperature dependence of thermoelectric power S for perovskites $Sr_{1-x}Pb_xRuO_3$ and $Sr_{1-z}Ca_zRuO_3$; all curves except $SrRuO_3$ were shifted vertically for clarification. (b) The thermoelectric power at room temperature versus x, y, and z for perovskites $Sr_{1-x}Pb_xRuO_3$, $Sr_{1-z}Ca_zRuO_3$, and $Sr_{1-y}Ba_yRuO_3$. Symbols of open triangle are for the Ba-substituted samples.

ments but occurs in the samples with compositions around the quantum critical point $x\approx 0.6$ where T_c goes to zero. This observation suggests that the thermoelectric power enhancement near 20 K may be due to quantum critical fluctuations (QCFs). Further verification of this argument will be done by measurements of thermoelectric power under a magnetic field. On the side of Ca substitution, T_c is also reduced and vanishes near $z=0.7$. Although a report has shown some quantum critical behavior associated with samples near $z=0.7$,[21] no enhancement like that on the side of Pb substitution is observed. However, a dramatic upturn of S at low temperatures in $CaRuO_3$ indicates that another QCP is approached, which supports a similar argument from the measurement of specific heat.[22]

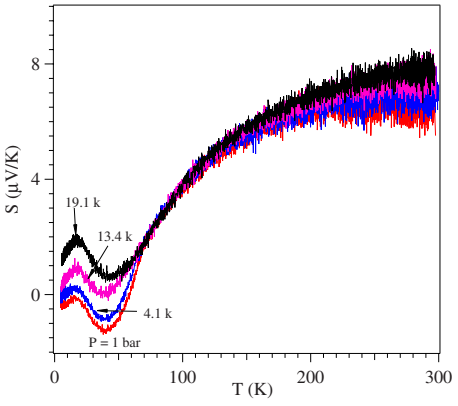

FIG. 10. (Color online) Temperature dependence of thermoelectric power S under high pressure for the perovskite $Sr_{0.05}Pb_{0.95}RuO_3$. Pressure labeled was measured at 250 K.

The magnitude of thermoelectric power at a given temperature is not directly related to the bandwidth but is determined by the unsymmetric energy-dependent conductivity around the Fermi energy.[23] However, for the isostructural single-valence system $ARuO_3$, the evolution of $|S|$ as a function of the tolerance factor t reflects the relative change in bandwidth. The thermoelectric power at room temperature as a function of Ca, Pb, and Ba substitutions are plotted in Fig. 9(b). S increases slightly on Ca substitution but drops much more steeply on Pb substitution. Pb substitution reduces S more dramatically than Ba substitution where the cubic phase $BaRuO_3$ with the highest symmetry in the system is reached. This plot indicates clearly that the orbital hybridization between Pb 6s and Ru 4d orbitals plays a more important role to broaden the bandwidth than the structural change in the Pb-substituted samples of $Sr_{1-x}Pb_xRuO_3$.

IV. CONCLUSIONS

The phase diagram of $Sr_{1-x}Pb_xRuO_3$ of Fig. 11 summarizes our major results. The orthorhombic perovskite structure with the *Pbnm* space group has been found in all Pb-substituted samples of $Sr_{1-x}Pb_xRuO_3$ to lowest temperatures, except in a narrow area below T_t near $PbRuO_3$ where a phase transition to another orthorhombic phase with the *Imma* space group takes place. The Pb substitution does not alter the metallic character of the conduction over the entire phase diagram, including both *Pbnm* and the *Imma* phases. The Curie temperature T_c in orthorhombic $SrRuO_3$ is gradually reduced as x increases in the system $Sr_{1-x}Pb_xRuO_3$ and eventually vanishes near $x=0.6$. All samples with compositions $x>0.6$ remain paramagnetic to lowest temperature. The influence of quantum critical fluctuations on transport properties at low temperatures has been observed in compositions near the quantum critical point $x\approx0.6$ and $x\approx0.9$. A comparison of the magnetic property and thermoelectric power between Pb- and Ba-substituted samples shows conclusively that the orbital hybridization between Pb 6s and Ru 4d plays an important role to suppress ferromagnetism in Pb-substituted samples.

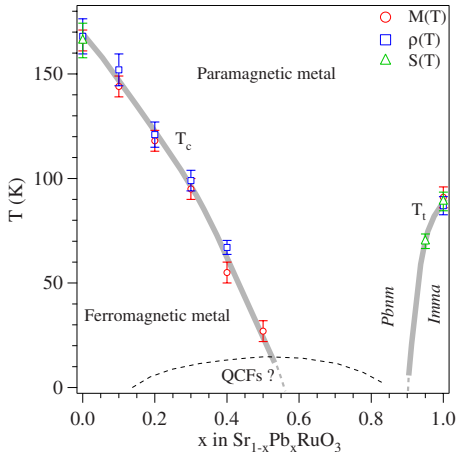

FIG. 11. (Color online) The phase diagram of perovskites $Sr_{1-x}Pb_xRuO_3$. Anomalous transport properties such as the extra enhancement in the thermoelectric power and non-Fermi-liquid behavior have been observed below the thin dashed line, that have been discussed in terms of QCFs as a quantum critical point near $x=0.6$ is approached, see text for the detail.

ACKNOWLEDGMENTS

This work was supported by NSF (Grant No. DMR 0904282) and the Robert A Welch foundation (Grant No. F-1066).

*jszhou@mail.utexas.edu

[1] E. P. Wohlfarth, J. Appl. Phys. **39**, 1061 (1968).
[2] T. Kiyama, K. Yoshimura, K. Kosuge, H. Mitamura, and T. Goto, J. Phys. Soc. Jpn. **68**, 3372 (1999).
[3] D. Kim, B. L. Zink, F. Hellman, S. McCall, G. Cao, and J. E. Crow, Phys. Rev. B **67**, 100406(R) (2003).
[4] J.-G. Cheng, J.-S. Zhou, and J. B. Goodenough (unpublished).
[5] C.-Q. Jin, J.-S. Zhou, J. B. Goodenough, Q. Q. Liu, J. G. Zhao, L. X. Yang, Y. Yu, R. C. Yu, T. Katsura, A. Shatskiy, and E. Ito, Proc. Natl. Acad. Sci. U.S.A. **105**, 7115 (2008).
[6] R. B. Griffiths, Phys. Rev. Lett. **23**, 17 (1969).
[7] S. A. J. Kimber, J. A. Rodgers, H. Wu, C. A. Murray, D. N. Argyriou, A. N. Fitch, D. I. Khomskii, and J. P. Attfield, Phys. Rev. Lett. **102**, 046409 (2009).
[8] J.-G. Cheng, J.-S. Zhou, and J. B. Goodenough, Phys. Rev. B **80**, 174426 (2009).
[9] J. A. Kafalas and J. M. Longo, Mater. Res. Bull. **5**, 193 (1970).
[10] H. Kobayashi, M. Nagata, R. Kanno, and Y. Kawamoto, Mater. Res. Bull. **29**, 1271 (1994).
[11] M. W. Lufaso and P. M. Woodward, Acta Crystallogr., Sect. B: Struct. Sci. **57**, 725 (2001).
[12] J.-S. Zhou and J. B. Goodenough, Phys. Rev. Lett. **94**, 065501 (2005).
[13] M. O'Keeffe and B. G. Hyde, Acta Crystallogr., Sect. B: Struct. Crystallogr. Cryst. Chem. **33**, 3802 (1977).
[14] C. J. Howard, K. S. Knight, B. J. Kennedy, and E. H. Kisi, J. Phys.: Condens. Matter **12**, L677 (2000).
[15] E. H. Mountstevens, J. P. Attfield, and S. A. T. Redfern, J. Phys.: Condens. Matter **15**, 8315 (2003).
[16] G. Cao, S. McCall, M. Shepard, J. E. Crow, and R. P. Guertin, Phys. Rev. B **56**, 321 (1997).
[17] T. He, Q. Huang, and R. J. Cava, Phys. Rev. B **63**, 024402 (2000).
[18] K. Yoshimura, T. Imai, T. Kiyama, K. R. Thurber, A. W. Hunt, and K. Kosuge, Phys. Rev. Lett. **83**, 4397 (1999).
[19] M. B. Salamon, P. Lin, and S. H. Chun, Phys. Rev. Lett. **88**, 197203 (2002).
[20] P. B. Allen, H. Berger, O. Chauvet, L. Forro, T. Jarlborg, A. Junod, B. Revaz, and G. Santi, Phys. Rev. B **53**, 4393 (1996).
[21] Y. Itoh, T. Mizoguchi, and K. Yoshimura, J. Phys. Soc. Jpn. **77**, 123702 (2008).
[22] G. Cao, O. Korneta, S. Chikara, L. DeLong, and P. Schlottmann, Solid State Commun. **148**, 305 (2008).
[23] H. Fritzsche, Solid State Commun. **9**, 1813 (1971).